First on-sky closed loop measurement and correction of atmospheric dispersion

Prashant Pathak[a], Olivier Guyon[a,c,d], Nemanja Jovanovic[a,f], Julien Lozi[a], F. Martinache[b], Y. Minowa[a], T. Kudo[a], H. Takami[e], Y. Hayano[e], and N. Narita[e,g,h]

[a]National Astronomical Observatory of Japan, Subaru Telescope, 650 North A'Ohoku Place, Hilo, HI, 96720, U.S.A.
[b]Observatoire de la Cote d'Azur, Boulevard de l'Observatoire, Nice, 06304, France
[c]Steward Observatory, University of Arizona, Tucson, AZ, 85721, U.S.A.
[d]College of Optical Sciences, University of Arizona, Tucson, AZ 85721, USA
[e]National Astronomical Observatory of Japan, 2-21-1 Osawa, Mitaka, Japan
[f]Department of Physics and Astronomy, Macquarie University, Sydney, NSW 2109, Australia
[g]Department of Astronomy, The University of Tokyo, 7-3-1 Hongo, Bunkyo-ku, Tokyo, 113-0033, Japan
[h]Astrobiology Center, 2-21-1 Osawa, Mitaka, Tokyo, 181-8588, Japan

ABSTRACT

In the field of exoplanetary sciences, high contrast imaging is crucial for the direct detection of, and answering questions about habitability of exoplanets. For the direct imaging of habitable exoplanets, it is important to employ low inner working angle (IWA) coronagraphs, which can image exoplanets close to the PSF. To achieve the full performance of such coronagraphs, it is crucial to correct for atmospheric dispersion to the highest degree, as any leakage will limit the contrast. To achieve the highest contrast with the state-of-the-art coronagraphs in the SCExAO instrument, the spread in the point-spread function due to residual atmospheric dispersion should not be more than 1 mas in the science band. In a traditional approach, atmospheric dispersion is compensated by an atmospheric dispersion compensator (ADC), which is simply based on model which only takes into account the elevation of telescope and hence results in imperfect correction of dispersion. In this paper we present the first on-sky closed-loop measurement and correction of residual atmospheric dispersion. Exploiting the elongated nature of chromatic speckles, we can precisely measure the presence of atmospheric dispersion and by driving the ADC, we can do real-time correction. With the above approach, in broadband operation (y-H band) we achieved a residual of 4.2 mas from an initial 18.8 mas and as low as 1.4 mas in H-band only after correction, which is close to our science requirement. This work will be valuable in the field of high contrast imaging of habitable exoplanets in the era of the ELTs.

Keywords: Adaptive Optics, Atmospheric dispersion, ADC, Exoplanets

1. INTRODUCTION

The field of exoplanetary science is still in the early stage of development, it started with the indirect detection of exoplanets and recently there have been numerous direct detections of exoplanets but the contribution is low compared to indirect detections. To answer questions about habitability of exoplanets, it is essential to utilize direct detection methods and be able to conduct spectroscopic studies. With advances in technology, direct detection of exoplanets is getting more robust and mature. High contrast instruments like Gemini Planet Imager (GPI)[1] and Spectro-Polarimetric High-contrast Exoplanet REsearch instrument (SPHERE),[2] have presented us with the direct detection of exoplanets,[3] which shows the scope and importance of direct imaging.

Further author information: (Send correspondence to P. Pathak), E-mail: prashant@naoj.org, Telephone: +01 808 934 5081

Adaptive Optics Systems V, edited by Enrico Marchetti, Laird M. Close, Jean-Pierre Véran, Proc. of SPIE Vol. 9909, 990956
 · doi: 10.1117/12.2234094

The basic architecture of a high contrast instrument employs extreme adaptive optics (ExAO) and coronagraphs to suppress the light coming from the host star to image companions in close proximity. High contrast instruments are able to deal with atmospheric turbulence using ExAO, achieving high Strehl ratio but the next most important error comes from atmospheric refraction, which limits achievable angular resolution and coronagraphic contrast. To image habitable planets close to the host star one needs to employ low IWA coronagraphs. The presences of refraction results in the spread of the PSF, which leads to leakage of light through small IWA coronagraphs, destroying the achievable contrast to image the exoplanets close to the host star.The requirement for previous generation high contrast instruments such as HiCIAO[4] was 1/30th of diffraction-limited PSF, however this was not achieved in practice. The latest high contrast instrument, the Subaru Coronagraphic Extreme Adaptive Optics (SCExAO) system,[5] which is constantly evolving with time by employing the latest technologies, will take us a step further in the field of direct imaging. The science requirement for SCExAO is a spread in the PSF of $< 1/50$th of the diffraction-limited PSF size, which translates to < 1 mas in the science band.

For correcting atmospheric refraction, an ADC is used, which consists of two prisms with similar refractive index material. The combination of two prisms is used to compensate for atmospheric dispersion by rotating the prisms with respect one another and rotating the entire assembly about the axis of propagation.[6] Traditionally, ADC's are based on a simple model of refraction from Earth's atmosphere, which only takes into account the elevation of the telescope, as the atmospheric refraction is the function of zenith angle. The problem with the current approach of correction is that it does not make any measurement of actual dispersion in the atmosphere and hence results in imperfect correction, leaving residual atmospheric dispersion. Several examples of model based ADC's include Keck[7] and Subaru[8] telescopes ADC's.

With advances in the technology, the speed and number of actuators in deformable mirrors (DM) has increased. These advances have enabled us to demonstrate multiple technological achievements on-sky including Speckle nulling,[9] improvements in the precision of astrometry and photometry[10] and in this case careful measurement and correction of residual atmospheric dispersion.

In this work, we present the first on-sky measurement and correction of residual atmospheric dispersion. Here we demonstrate that by using an adaptive speckle grid, we can accurately measure the residual atmospheric dispersion and subsequently correct it to ≈ 1 mas in H-band. In section 2 and 3, we show the concept and its implementation using simulation and section 4 presents the on-sky results.

2. PRINCIPLE

When light from an astronomical object crosses the boundary of the vacuum of the space and the Earth's atmosphere it gets refracted in a manner akin to a prism. Refraction is a function of the wavelength, and shorter wavelength undergo more refraction compared to the longer wavelength. For a certain bandwidth observation, the presence of atmospheric refraction will induce elongation in the PSF and thus spread the PSF, which forms a dispersion vector, shown as $\vec{\mathbf{s}}$ in Figure 1. The magnitude of the dispersion vector is proportional to the atmospheric refraction, which is a function of the zenith angle (elevation of the telescope), as a result dispersion increases with the increase in the zenith angle. To cancel elongation in the PSF, an Atmospheric Dispersion Compensator (ADC) is used, which consists of two prisms with similar dispersion magnitude to minimize the asymmetric aberrations. The ADC dispersion vector $\vec{\mathbf{a}}$ is the sum of the two individual prisms dispersion vectors, as shown in Equation 1. Two prisms give maximum dispersion when individual vectors are at zero degree (co-aligned) with each other and minimum when they are 180 degree (anti-aligned). For more details of how an ADC operates please see.[8]

Currently ADC operation is based on the model of the known refractive index of the atmosphere and the zenith angle or angle of incidence on the Earth's atmosphere. This simplistic model corrects the majority of the atmospheric atmosphere dispersion but some residual or imperfection remain. Because of the incomplete compensation, we are left with the residual atmospheric dispersion vector $\vec{\mathbf{r}}$ as shown in Figure 1, which is the sum of the vectors $\vec{\mathbf{s}}$ and $\vec{\mathbf{a}}$, as shown in Equations 4 and 5. Below we show that, if we can measure the residual dispersion on-sky, we can correct for it in real-time.

The ADC dispersion vector $\vec{\mathbf{a}}$ is the sum of $\vec{\mathbf{p1}}$ and $\vec{\mathbf{p2}}$, represented by Equation 1. Individual prism dispersion vectors are shown in Equations 2 and 3, in terms of x and y coordinates (physical coordinates), where $\mathbf{p}$ is the

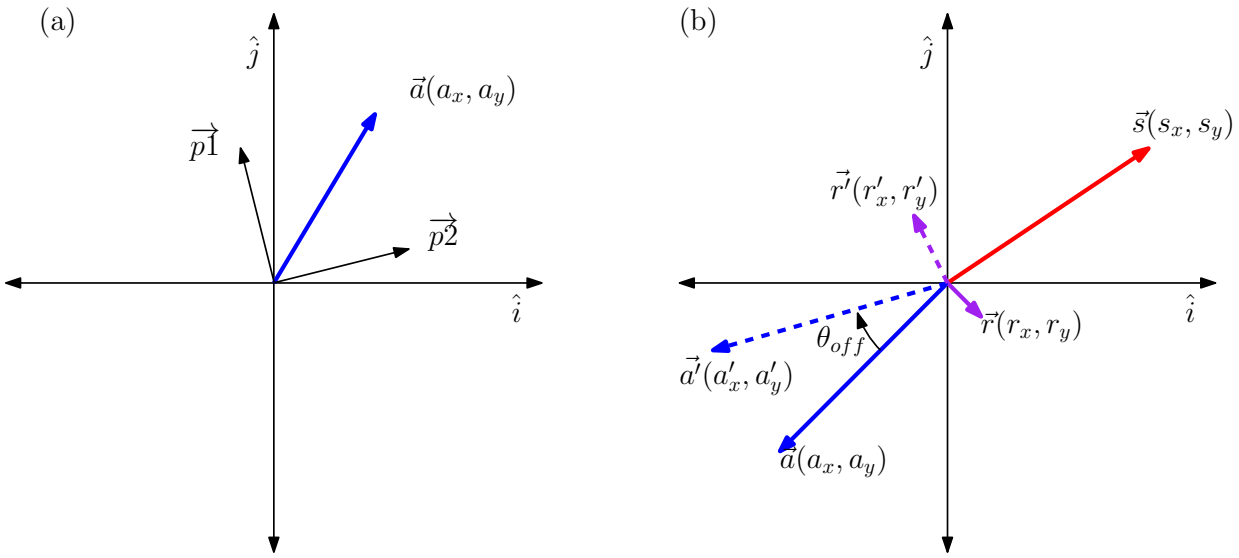

Figure 1. Schematic showing the function of the ADC (Atmospheric Dispersion Compensator): (a) ADC vector $\vec{\mathbf{a}}$ is sum of prism vectors $\vec{\mathbf{p1}}$ and $\vec{\mathbf{p1}}$. (b) This schematic shows working of the ADC, the dispersion vector $\vec{\mathbf{s}}$ is canceled by the ADC vector $\vec{\mathbf{a}}$ and the residual vector is given by $\vec{\mathbf{r}}$.

dispersion magnitude of each prism and θ_1 and θ_2 are prism orientation angles.

$$\vec{a} = \overrightarrow{p1} + \overrightarrow{p2} \tag{1}$$
$$\overrightarrow{p1} = p\cos(\theta_1)\hat{i} + p\sin(\theta_1)\hat{j} \tag{2}$$
$$\overrightarrow{p2} = p\cos(\theta_2)\hat{i} + p\sin(\theta_2)\hat{j} \tag{3}$$

So the x and y component of the ADC vector is given by:

$$a_x = p\cos(\theta_1) + p\cos(\theta_2)$$
$$a_y = p\sin(\theta_1) + p\sin(\theta_2)$$

The sum of vectors $\vec{\mathbf{s}}$ and $\vec{\mathbf{a}}$ in terms of x and y component is shown below,

$$s_x + a_x = r_x \tag{4}$$
$$s_y + a_y = r_y \tag{5}$$

If we assume for a short period of time, the on-sky dispersion vector $\vec{\mathbf{s}}$ does not change and we rotate the ADC vector by angle θ_{off} (offset orientation angle), we get a new ADC vector $\vec{\mathbf{a'}}$ shown below,

$$a'_x = p\cos(\theta_1 - \theta_{off}) + p\cos(\theta_2 - \theta_{off}) \tag{6}$$
$$a'_y = p\sin(\theta_1 - \theta_{off}) + p\sin(\theta_2 - \theta_{off}) \tag{7}$$

Now by adding vectors $\vec{\mathbf{s}}$ and $\vec{\mathbf{a'}}$, we get a new residual dispersion vector $\vec{\mathbf{r'}}$, which is decomposed into individual Equation 8 and 9:

$$s_x + a'_x = r'_x \tag{8}$$
$$s_y + a'_y = r'_y \tag{9}$$

By subtracting equation 8 from 4 and 9 from 5 we get:

$$a_x - a'_x = r_x - r'_x \tag{10}$$
$$a_y - a'_y = r_y - r'_y \tag{11}$$

Now substituting the values of a_x, a'_x, a_y and a'_y into Equation 10 and 11, we get:

$$p \times l = r_x - r'_x \tag{12}$$
$$p \times m = r_y - r'_y \tag{13}$$

where l and m are,

$$l = \cos(\theta_1) + \cos(\theta_2) - \cos(\theta_1 - \theta_{off}) - \cos(\theta_2 - \theta_{off})$$
$$m = \sin(\theta_1) + \sin(\theta_2) - \sin(\theta_1 - \theta_{off}) - \sin(\theta_2 - \theta_{off})$$

In Equations 12 and 13, θ_1 and θ_2 are the initial prism angles, θ_{off} is the offset applied to the prisms and (r_x, r_y) and (r'_x, r'_y) are component of measured residual dispersion vector before and after the offset is applied to the prisms, by putting all these parameters into Equation 14, the magnitude of the prism dispersion vector $\mathbf{p}$ can be calculated.

$$p = \left(\frac{(r_x - r'_x)^2 + (r_y - r'_y)^2}{l^2 + m^2} \right)^{\frac{1}{2}} \tag{14}$$

By knowing $\mathbf{p}$, one can calculate vector $\vec{\mathbf{a}}$ using Equation 1 and then on-sky dispersion vector $\vec{\mathbf{s}}$ can be calculated using ADC and residual vectors $\vec{\mathbf{a}}$ and $\vec{\mathbf{r}}$ as explained in Equations 4 and 5. Once we know the on-sky dispersion vector $\vec{\mathbf{s}}$, we can rotate the prisms in the appropriate directions to get rid of the residual dispersion.

3. SIMULATION

The above equations show that, if we can measure the residual dispersion, then it can be corrected by driving the ADC to the correct position. The idea behind measuring residual dispersion is to use the property of diffraction. Suppose we have visible light with no dispersion and each wavelength of light is focused at the center. When the central spot is diffracted vertically and horizontally, it splits into different colors, shorter wavelengths closer to the central spot and longer wavelengths farther, as shown in the Figure 2, (a). When there is no dispersion the line joining the diffracted spots (speckles) intersects at the center. When there is dispersion, the line joining the speckles does not meet at the central spot, as shown in Figure 2, (b). By measuring the distance between the intersection of the line joining the speckles and the central spot, the presence of dispersion can be measured indirectly. To test the above concept, simulations carried out to verify this. For the simulations the Subaru telescope pupil geometry was taken into consideration, as you can see in Figure 3, (a), which shows the pupil geometry of Subaru with the correct plate scale matched to the internal science camera in SCExAO. In Figure 3 (b), the corresponding PSF for the pupil geometry is shown, which was calculated by taking the Fourier transform of the pupil. To simulate multiple-wavelengths ie broadband operation y-H band in this case, the pupil size was varied and Fourier transforms of each pupil were calculated and the corresponding PSF's were over-lapped to create a multi-wavelength PSF. Figure 3, (c), was generated by putting a sinusoidal modulation in the pupil in x and y axis, which acts as a grating and diffracts the PSF, in this simulation there is no atmospheric dispersion present. Figure 3, (d), was generated in a similar way to (c) with the addition of dispersion. In this simulation, as you can see, the speckles don't point towards the PSF anymore.

3.1 Measuring Atmospheric Disperion

Naturally the first approach was to fit lines to the speckles using a Gaussian fit but the varying intensity of real speckles in experiment made it difficult to find a precise point of intersection, in addition to water absorption between J and H-band, which is clearly visible in the speckles of Figure 7, which causes discontinuity in the speckles. Therefore a technique that involved cross-correlating speckles, which was robust to these noise sources was used. The details of the method used is explained using the schematic in Figure 4, (a) which shows the PSF and speckles in the presence of atmospheric dispersion, it also shows the radiation center, which is the point where speckles meet if elongated. Figure 4 (b) shows speckles only with the PSF removed, blue speckles represent the original speckle and red speckles are generated by radial stretch of the blue speckles about the PSF center. Figure 4 (c) was generated in similar way to (b), except the point of radial stretch is now the radiation center.

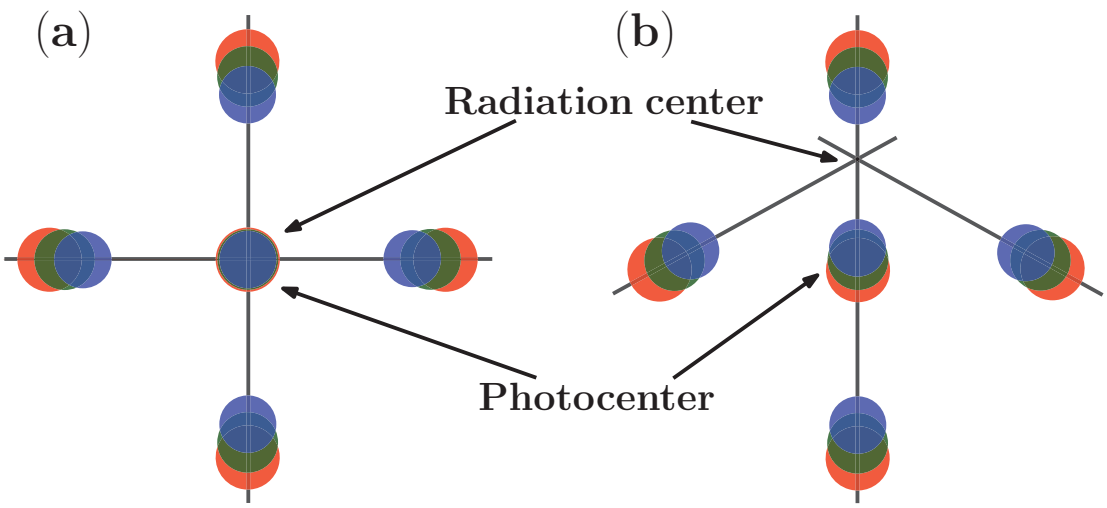

Figure 2. Schematic shows the concept behind the measurement of atmospheric dispersion, central spot consists of visible spectrum, which is diffracted to generate speckles. (a) When there is no atmospheric dispersion, each wavelength of light is focused at the center and the line joining the chromatic speckles meet at the center. (b) When there is atmospheric dispersion, line joining the speckles does not meet at the center.

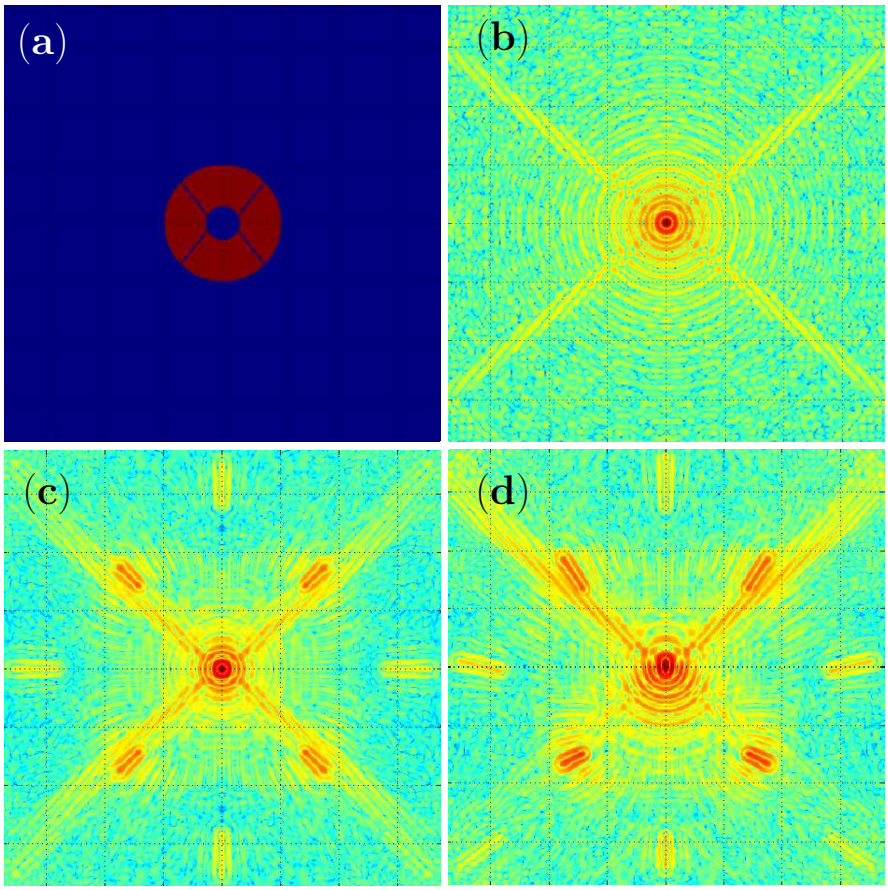

Figure 3. (a) Subaru telescope pupil geometry. (b) PSF corresponding to the pupil. (c) Diffracted PSF with no atmospheric dispersion present. (d) Diffracted PSF with atmospheric dispersion.

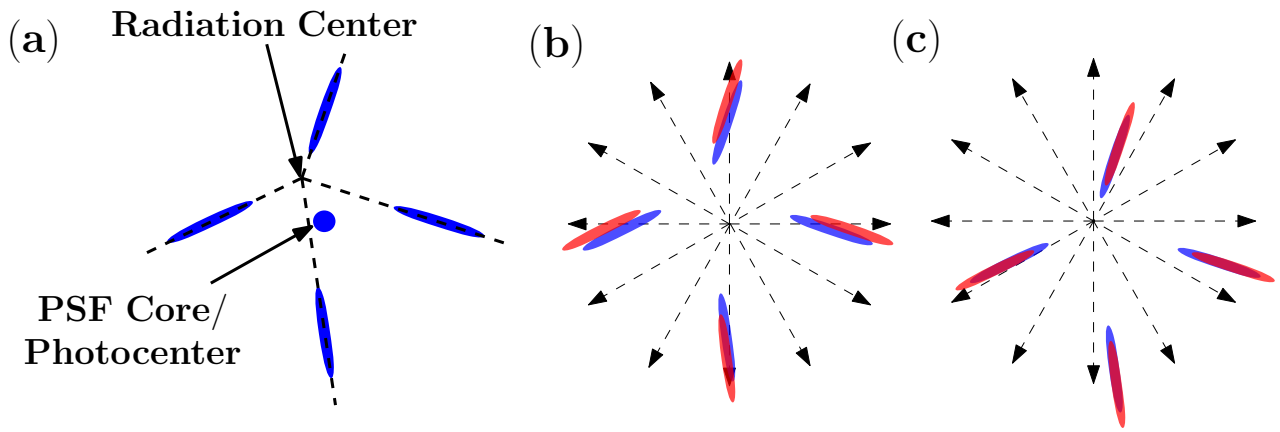

Figure 4. (a) Shows the PSF and speckles with the presence of atmospheric dispersion, it also shows the radiation center, which the is point where the speckles meet if elongated. (b) Speckle only image from above, blue speckles represent original speckle and red represents radially stretched speckles from the PSF center. (c) same schematic as in (b), except point of radial zoom is radiation center.

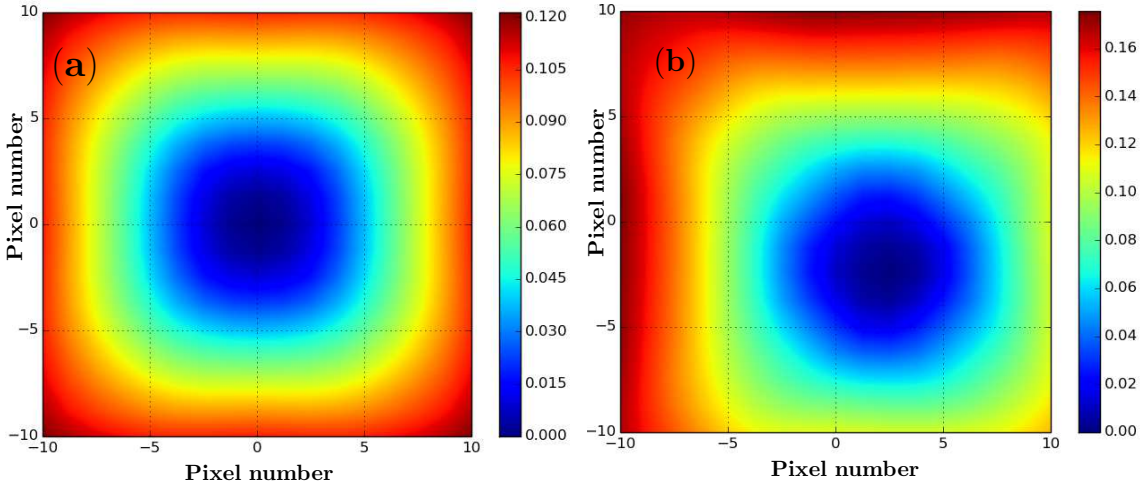

Figure 5. Shows the result of cross-correlation on simulated PSF.

These schematics show that, if the radial stretch is from the radiation center, the original and stretched speckles overlap and subtracting the two will lead to the minimization of the residual flux in the image. So to find the center of radiation, the PSF was first subtracted from the image then a raster scan was conducted around the region of the PSF center, in each case the residual flux in the frame after the subtraction of the speckles from the stretched image was recorded. The result of such an analysis is shown in Figure 5, the minimum represents the radiation center, while the center of the image represents the location of PSF center. The closer the minimum lies to the center, the less dispersion that is present. To find the minimum with sub-pixel accuracy, the contour plot was interpolated. Figure 5 (a), show the cross-correlation result for a PSF which does not have atmospheric dispersion, and hence the minimum is at the center. Figure 5 (b), shows the cross-correlation result of a PSF with dispersion, which shows a minimum away from the center. With the aid of simulation, it was found that the relationship between applied dispersion and distance between PSF and radiation center is in the ratio of 1:2, this relationship is later used to calculate the on-sky dispersion in section 4. By this method one can indirectly measure the residual dispersion to sub-pixel accuracy.

3.2 ADC Simulation

The operation of an ADC was simulated to test the measurement and correction of dispersion on a simulated PSF. As you can see in Figure 6, the first part of the simulation involves calibration of the ADC. The inputs used

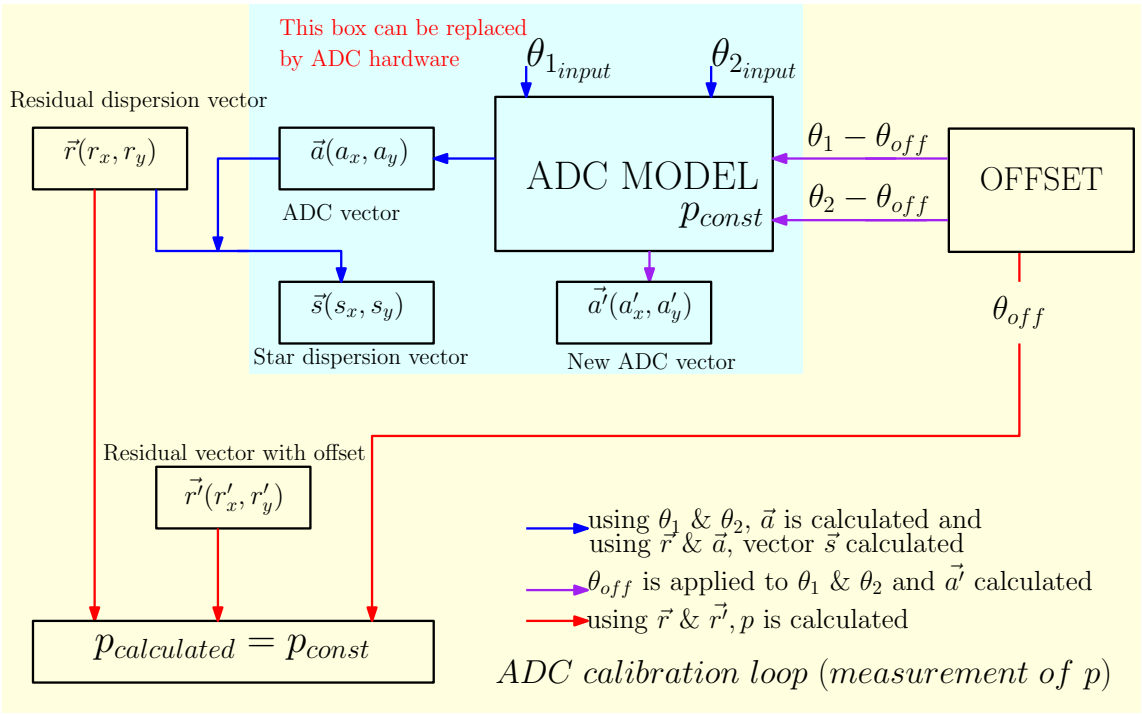

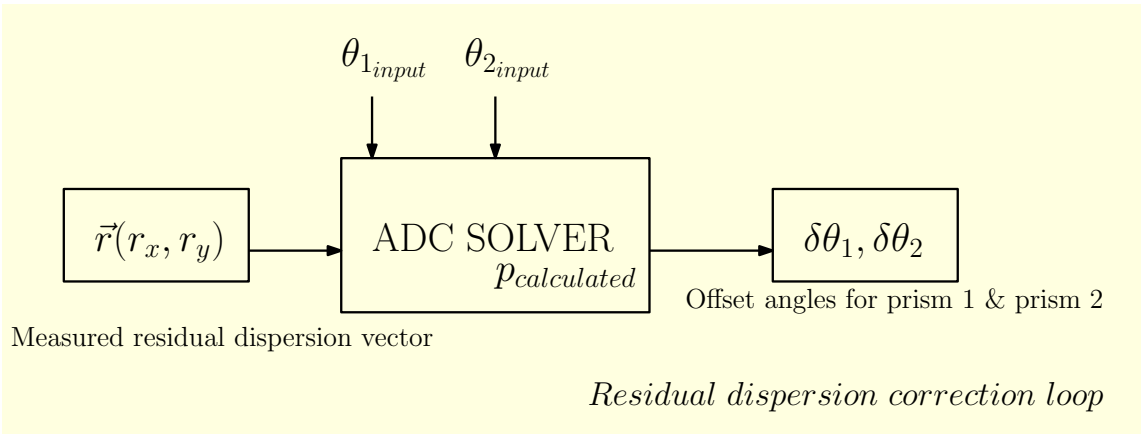

Figure 6. Schematic of the control loop, used for calibration of the ADC and calculating the offset angles of the prisms, for correcting atmospheric dispersion.

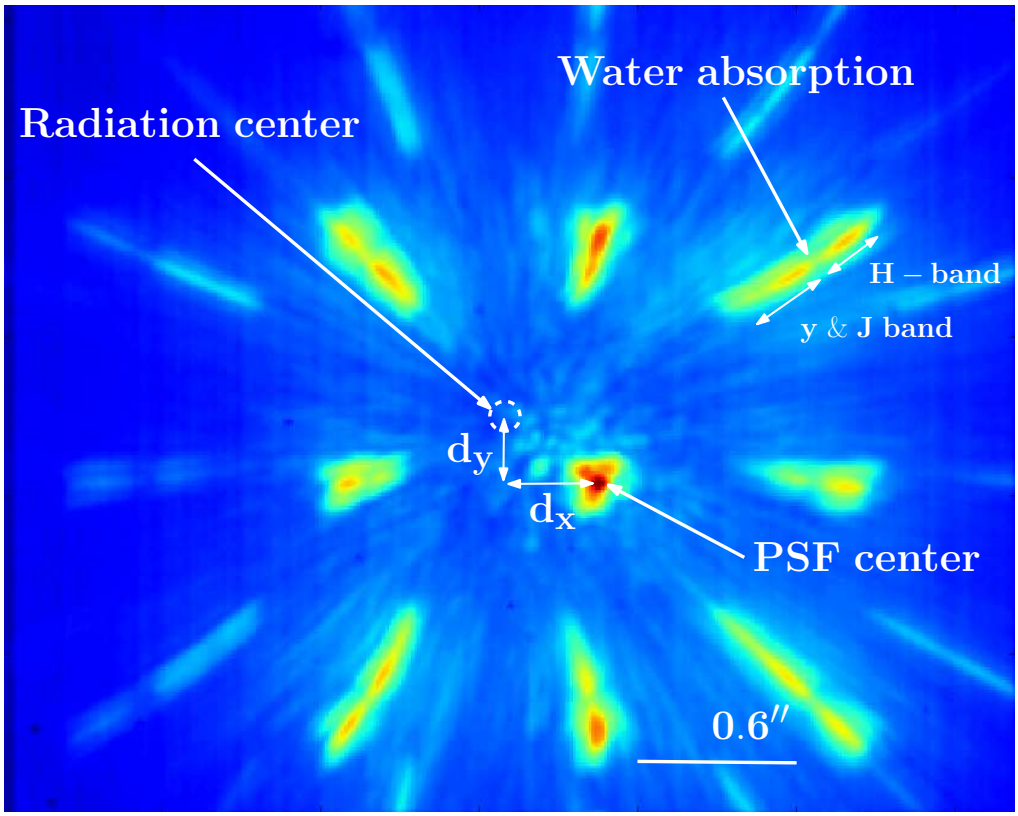

Figure 7. On-sky PSF, showing radiation and PSF center. Deviation of radiation center from PSF shows presence of atmospheric dispersion.

in simulation are prism angles θ_1 and θ_2 and the magnitude of prism dispersion vector $\mathbf{p}$, which is an unknown constant. By using these parameters the ADC vector $\vec{\mathbf{a}}$ is calculated, for details of equations used here refer to section 2. And using vectors $\vec{\mathbf{r}}$ and$\vec{\mathbf{a}}$, on-sky dispersion vector $\vec{\mathbf{s}}$ is calculated. In the second step: offset is applied to θ_1 and θ_2 by θ_{off}, which gives the new ADC vector $\vec{\mathbf{a}'}$ and residual vector $\vec{\mathbf{r}'}$. And by using residual vectors $\vec{\mathbf{r}}$, $\vec{\mathbf{r}'}$ and offset angle θ_{of}, prism dispersion magnitude $\mathbf{p}$ can be calculated. In the second part of the simulation using the measured residual dispersion vector $\vec{\mathbf{r}}$, the prism angles and $\mathbf{p_{calculated}}$, offset angles $\delta\theta_1$ and $\delta\theta_2$ are calculated, which will give us a better correction of dispersion.

4. RESULTS

As explained in the papers Jovanovic et. al.[10] and Frantz et. al.,[9] artificial speckles can be generated by diffracting the PSF using a DM having a large number of actuators. In this case the SCExAO DM was used, which has 45 actuators across the pupil and they can be modulated to create a grating like structure in the form of a sine wave. The distance between the PSF and speckles is a function of the number of sine waves across the pupil, more cycles across pupil, the further a speckle is projected from the PSF and vice versa. For a 45 actuator DM, the furthest speckles can be placed is 22.5 λ/D from the PSF (Jovanovic et al. 2015). The brightness of the speckles can be controlled by adjusting the amplitude of the sine wave. On-sky speckles were placed at 22.5 λ/D, with a 100 nm RMS amplitude for each sine wave on DM. Image were taken using the internal near infra-red (NIR) camera (320×256 InGaAs). The target was Beta Leo (spectral type A3, R-mag = 2.08, H-mag = 1.92) on the SCExAO engineering night of the 2015 April 2^{nd}. The data was collected using AO188, which is the Subaru Telescope facility AO instrument with loop closed, it offers Strehl between $20-40\%$, for more detail refer.[11] The capture elongated speckles a broadband filter y-H band was placed in front of the camera. For image processing, a mean dark frame was calculated from a cube of 1000 dark frames, which was subtracted from science images and hot pixels were removed. The telescope elevation was 43° and ADC correction was not

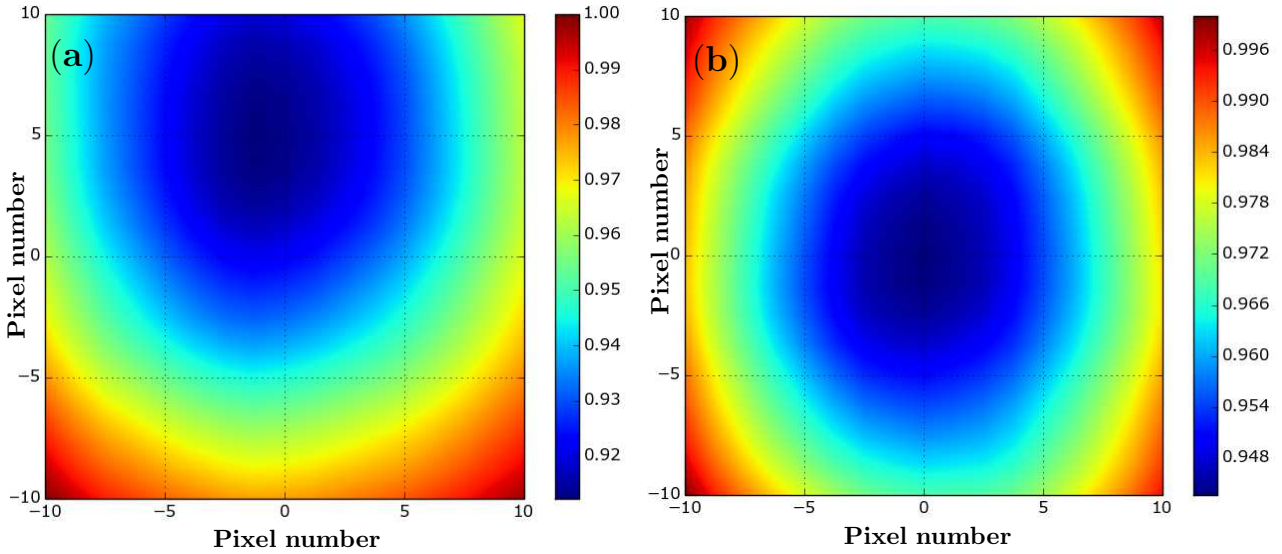

Figure 8. On-sky result with contour plot, showing the position of radiation center. (a) Before correcting the residual atmospheric dispersion. (b) After correcting the residual atmospheric dispersion.

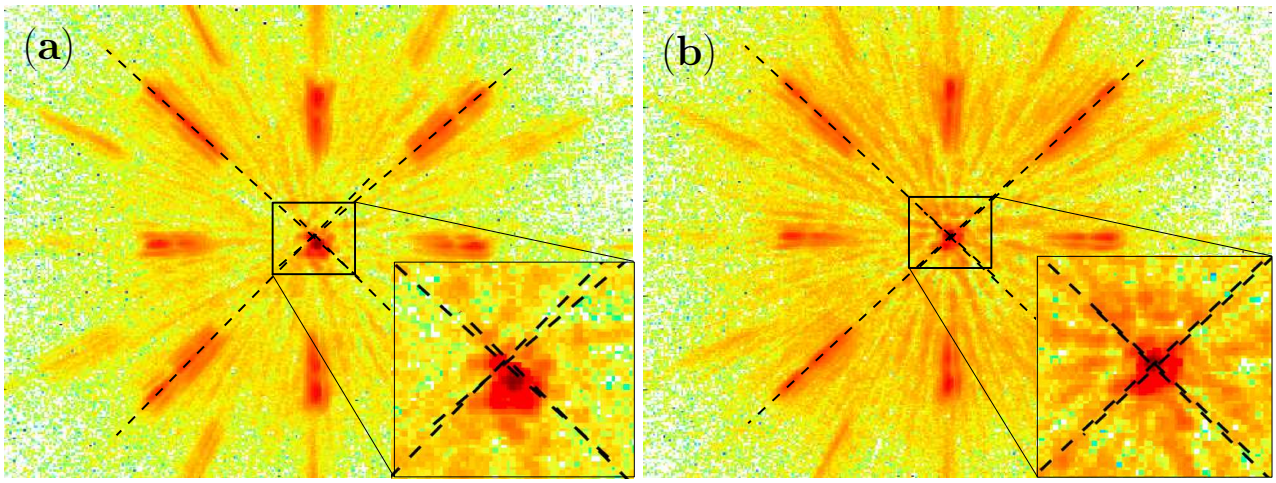

Figure 9. PSF with speckles, (a) before correcting the residual atmospheric dispersion: lines are over-plotted to show radiation center does not coincide with PSF center. (b) After correcting the residual dispersion: over-plotted lines shows radiation center coincides with the PSF center.

applied to highlight the presence of atmospheric dispersion. As shown in Figure 7, the speckles do not point to the PSF center as expected. The on-sky correction of residual atmospheric dispersion was achieved on the target Alpha Ari (spectral type K1, R-mag = 1.15, H-mag = -0.52) on the SCExAO engineering night of the October 30^{th} 2015, using the same specifications as explained above. The results of the on-sky measurement and correction of residual atmospheric dispersion is shown in the Figure 9. Figure 9 (a), shows speckles and the PSF, with superimposed lines to show the intersection point lies away the PSF center. Figure 9 (b), shows speckles after correcting for residual dispersion, here the intersection point lies close to the PSF center. For finding the radiation center, the method explained in the section 3.1 was used and the results are shown in Figure 8. In Figure 8 (a) the radiation center lies above the PSF which is before correction and (b) represents the result after correction, where the radiation center is close to center. The results from, cross-correlation are summarized in Table 1, Values of d_x and d_y shown in the table, represent distance of radiation center from the PSF, in dispersion unit ($\mu as/nm$) converted from pixel values (for internal science camera 1 pixel = 12.1 mas). The values of d_x and d_y are then converted to spread in PSF by the relationship between distance and dispersion as explained

in section 3. As you can see in the table we have reduced residual atmospheric dispersion from 20.9 $\mu as/nm$ to 4.7 $\mu as/nm$, which corresponds to 4.7 mas in the y-H band and 1.4 mas in H-band alone, which is close to our science requirement (1 mas in H-band). These results show the scope of this work in improving the ground based high contrast imaging for direct detection of habitable exoplanets.

Table 1. Residual Atmospheric Dispersion ($\mu as/nm$)

	d_x	d_y	PSF spread
	mas	mas	μas/nm
Without Correction	-3.6 ± 8.3	41.6 ± 8.0	20.9
With Correction	7.7 ± 6.5	-5.3 ± 8.4	4.7

5. SUMMARY

In this work, we demonstrate the first on-sky measurement and correction of residual atmospheric dispersion using an adaptive speckle grid.

This technique can be used by other AO systems, which do not employ high actuator DM's to create speckle grids, by using a diffractive grid in the pupil. This concept will be extended to work in conjunction with coronagraphs, where the location of the PSF behind the coronagraph can be found by cross-correlating the speckles in the grid. In this work, we have canceled one leading noise term which prevents direct imaging of habitable planets. This work will be valuable in the field of ground based high contrast imaging of habitable exoplanets in the era of ELT's, because it shows the path to correct atmospheric dispersion to the highest degree compared to traditional approaches. It can also be incorporated in atmospheric dispersion corrector design for ELT's.[12]

REFERENCES

[1] Macintosh, B., Graham, J. R., and Ingraham, Patrick, e. a., "First light of the gemini planet imager," *Proceedings of the National Academy of Sciences* **111**(35), 12661–12666 (2014).

[2] Beuzit, J.-L., Feldt, M., Dohlen, K., Mouillet, D., Puget, P., Wildi, F., Abe, L., Antichi, J., Baruffolo, A., Baudoz, P., Boccaletti, A., Carbillet, M., Charton, J., Claudi, R., Downing, M., Fabron, C., Feautrier, P., Fedrigo, E., Fusco, T., Gach, J.-L., Gratton, R., Henning, T., Hubin, N., Joos, F., Kasper, M., Langlois, M., Lenzen, R., Moutou, C., Pavlov, A., Petit, C., Pragt, J., Rabou, P., Rigal, F., Roelfsema, R., Rousset, G., Saisse, M., Schmid, H.-M., Stadler, E., Thalmann, C., Turatto, M., Udry, S., Vakili, F., and Waters, R., "Sphere: a 'planet finder' instrument for the vlt," (2008).

[3] Macintosh, B., Graham, J. R., Barman, T., De Rosa, R. J., Konopacky, Q., Marley, M. S., Marois, C., Nielsen, E. L., Pueyo, L., Rajan, A., Rameau, J., Saumon, D., Wang, J. J., Patience, J., Ammons, M., Arriaga, P., Artigau, E., Beckwith, S., Brewster, J., Bruzzone, S., Bulger, J., Burningham, B., Burrows, A. S., Chen, C., Chiang, E., Chilcote, J. K., Dawson, R. I., Dong, R., Doyon, R., Draper, Z. H., Duchêne, G., Esposito, T. M., Fabrycky, D., Fitzgerald, M. P., Follette, K. B., Fortney, J. J., Gerard, B., Goodsell, S., Greenbaum, A. Z., Hibon, P., Hinkley, S., Cotten, T. H., Hung, L.-W., Ingraham, P., Johnson-Groh, M., Kalas, P., Lafreniere, D., Larkin, J. E., Lee, J., Line, M., Long, D., Maire, J., Marchis, F., Matthews, B. C., Max, C. E., Metchev, S., Millar-Blanchaer, M. A., Mittal, T., Morley, C. V., Morzinski, K. M., Murray-Clay, R., Oppenheimer, R., Palmer, D. W., Patel, R., Perrin, M. D., Poyneer, L. A., Rafikov, R. R., Rantakyrö, F. T., Rice, E. L., Rojo, P., Rudy, A. R., Ruffio, J.-B., Ruiz, M. T., Sadakuni, N., Saddlemyer, L., Salama, M., Savransky, D., Schneider, A. C., Sivaramakrishnan, A., Song, I., Soummer, R., Thomas, S., Vasisht, G., Wallace, J. K., Ward-Duong, K., Wiktorowicz, S. J., Wolff, S. G., and Zuckerman, B., "Discovery and spectroscopy of the young jovian planet 51 eri b with the gemini planet imager," *Science* **350**(6256), 64–67 (2015).

[4] Hodapp, K. W., Suzuki, R., Tamura, M., Abe, L., Suto, H., Kandori, R., Morino, J., Nishimura, T., Takami, H., Guyon, O., Jacobson, S., Stahlberger, V., Yamada, H., Shelton, R., Hashimoto, J., Tavrov, A., Nishikawa, J., Ukita, N., Izumiura, H., Hayashi, M., Nakajima, T., Yamada, T., and Usuda, T., "Hiciao: the subaru telescope's new high-contrast coronographic imager for adaptive optics," (2008).

[5] Jovanovic, N., Martinache, F., Guyon, O., Clergeon, C., Singh, G., Kudo, T., Garrel, V., Newman, K., Doughty, D., Lozi, J., Males, J., Minowa, Y., Hayano, Y., Takato, N., Morino, J., Kuhn, J., Serabyn, E., Norris, B., Tuthill, P., Schworer, G., Stewart, P., Close, L., Huby, E., Perrin, G., Lacour, S., Gauchet, L., Vievard, S., Murakami, N., Oshiyama, F., Baba, N., Matsuo, T., Nishikawa, J., Tamura, M., Lai, O., Marchis, F., Duchene, G., Kotani, T., and Woillez, J., "The subaru coronagraphic extreme adaptive optics system: Enabling high-contrast imaging on solar-system scales," *Publications of the Astronomical Society of the Pacific* **127**(955), 890 (2015).

[6] Allen, C. V., [*Astrophysical Quantities*], The Athlone Press, London and Atlantic Highlands (1997 (third edition)).

[7] Wynne, C. G., "Correction of atmospheric dispersion in the infrared," *mnras* **282**, 863–867 (oct 1996).

[8] Egner, S., Ikeda, Y., Watanabe, M., Hayano, Y., Golota, T., Hattori, M., Ito, M., Minowa, Y., Oya, S., Saito, Y., Takami, H., and Iye, M., "Atmospheric dispersion correction for the subaru ao system," (2010).

[9] Martinache, F., Guyon, O., Jovanovic, N., Clergeon, C., Singh, G., Kudo, T., Currie, T., Thalmann, C., McElwain, M., and Tamura, M., "On-sky speckle nulling demonstration at small angular separation with scexao," *Publications of the Astronomical Society of the Pacific* **126**(940), 565 (2014).

[10] Jovanovic, N., Guyon, O., Martinache, F., Pathak, P., Hagelberg, J., and Kudo, T., "Artificial incoherent speckles enable precision astrometry and photometry in high-contrast imaging," *The Astrophysical Journal Letters* **813**(2), L24 (2015).

[11] Minowa, Y., Hayano, Y., Oya, S., Watanabe, M., Hattori, M., Guyon, O., Egner, S., Saito, Y., Ito, M., Takami, H., Garrel, V., Colley, S., Golota, T., and Iye, M., "Performance of subaru adaptive optics system ao188," (2010).

[12] Bahrami, M. and Goncharov, A. V., "The achromatic design of an atmospheric dispersion corrector for extremely large telescopes," *Optics Express* **19**, 17099–17113 (Aug. 2011).